Chemical Geology 356 (2013) 64–75

Contents lists available at ScienceDirect

Chemical Geology

journal homepage: www.elsevier.com/locate/chemgeo

Magnesium-isotope and REE compositions of Lower Ordovician carbonates from eastern Laurentia: Implications for the origin of dolomites and limestones

Karem Azmy [a,*], Denis Lavoie [b], Zhengrong Wang [c], Uwe Brand [d], Ihsan Al-Aasm [e], Simon Jackson [f], Isabelle Girard [f]

[a] Department of Earth Sciences, Memorial University of Newfoundland, St. John's, NL A1B 3X5, Canada
[b] Geological Survey of Canada, GSC-Q, Natural Resources Canada, 490 de la Couronne, Québec, Qc G1K 9A9, Canada
[c] Department of Geology and Geophysics, Yale University, New Haven, CT 06520-8109, USA
[d] Department of Earth Sciences, Brock University, St. Catharines, ON L2S 3A1, Canada
[e] Department of Earth and Environmental Sciences, University of Windsor, Windsor, Ontario N9B 3P4, Canada
[f] Geological Survey of Canada, Natural Resources Canada, 601 rue Booth St., Ottawa, Ontario K1A 0E8, Canada

ARTICLE INFO

Article history:
Received 14 February 2013
Received in revised form 16 July 2013
Accepted 17 July 2013
Available online 27 July 2013

Editor: David R. Hilton

Keywords:
Lower Ordovician
St. George Group dolomites
Modern bulk sabkha sediments (dolomites)
Mg-isotopes
Source characterization
REE

ABSTRACT

Carbonates representing different depositional and diagenetic settings (near-surface to deep burial), including modern sabkha, were collected from the Lower Ordovician St. George Group in eastern Laurentia (western Newfoundland, Canada). Based on petrographic examination, three dolomite phases were identified: D1 dolomicrite (crystals ranging from 4 to 50 μm), D2 dolomite (50 to 150 μm) and D3 saddle dolomite (≥500 μm). They occur as replacements and cements, and exhibit dull (for D1 and D3) to zoned (for D2) luminescence. The occurrence of near-micritic dolomites (D1) suggests that dolomitization started at low temperatures under near-surface conditions during an early stage of diagenesis, whereas microthermometric studies of the D2 and D3 dolomites confirmed their formation at higher temperatures, on average, of 112 ± 19 °C and 153 ± 30 °C, respectively, under deeper burial conditions.

The D1 dolomicrite yields an average δ^{26}Mg value of −1.92 ± 0.30‰ (DSM3), which is slightly more negative than those of the D2 dolomite with −1.75 ± 0.34‰ (DSM3) and D3 saddle dolomite with −1.58 ± 0.31‰ (DSM3). The slightly more positive δ^{26}Mg values of the higher-temperature dolomites (D2 and D3) suggest insignificant kinetic fractionation and slight overprinting by ^{26}Mg-enriched diagenetic fluids recirculating in siliciclastic and ^{26}Mg-rich crustal rocks under closed to semi-closed diagenetic conditions.

The Sr-isotope signatures support the formation of D1 dolomicrite in an early diagenetic stage and the REE compositions of the investigated dolomites favor their formation in semi-closed to closed diagenetic systems with fluid compositions evolving by circulation through crustal rocks with progressive burial. Furthermore, the Mg isotopes suggest that the lime mudstones of the St. George Group had an algal origin, whereas the D2 dolomite was sourced and subsequently altered mostly from the D1 dolomicrites of the succession.

1. Introduction

Dolomites constitute significant hydrocarbon reservoirs and the origin of associated hydrothermal dolomites has, therefore, become an increasing focus of studies. Despite intensive research, including modeling (e.g., Azmy et al., 2009) and fluid inclusion studies (e.g., Conliffe et al., 2010), the influence of the diagenetic environment and evolution of fluid chemistry on dolomitization is still hotly debated. A novel approach to understanding the depositional and diagenetic controls on the composition of dolomites is the investigation of their Mg-isotope compositions since the replacement of Ca^{2+} by Mg^{2+} and type of dolomite are strongly related to the diagenetic environment (e.g., Budd, 1997; Warren, 2000), and possibly their original source. The Mg isotope composition of dolomites and its relationship to conditions of burial may shed some light on the origin of dolomitizing fluids and controls on Mg-isotopic fractionation during dolomitization (e.g., Lavoie et al., 2010). Although some recent investigations reported discrete differences in Mg isotope compositions of terrestrial silicate rocks and carbonate sediments, much more research into their distribution is needed (e.g., Galy et al., 2002; Chang et al., 2003; Carder et al., 2004; De Villiers et al., 2005; Tipper et al., 2006a; Hippler et al., 2009; Immenhauser et al., 2010; Wombacher et al., 2011; Huang et al., 2013; Wang et al., 2013).

* Corresponding author.
E-mail address: kazmy@mun.ca (K. Azmy).

0009-2541/$ – see front matter © 2013 Elsevier B.V. All rights reserved.
http://dx.doi.org/10.1016/j.chemgeo.2013.07.015

The main objective of our study is to utilize the Mg-isotope signatures of the paragenetically and geochemically well-constrained limestone and dolomite-rich succession of the Lower Ordovician St. George Group (Newfoundland, Canada) to better understand the genesis of dolomites formed under different diagenetic settings. This is an attempt to trace the origin of dolomitizing fluids and the source of Mg in the fluids, and to understand the fractionation behavior of Mg isotopes during shallow to deep burial. It is envisaged that Mg isotopes may have great potential for better understanding the still elusive process of dolomitization. Furthermore, the Mg isotopes may aid in the characterization and identification of the sources and precursors of the studied carbonates.

2. Geologic setting and lithostratigraphy

The Lower Ordovician St. George Group in western Newfoundland, Canada (Fig. 1) consists of tropical, shallow water carbonates that were deposited on a wide, peritidal carbonate ramp (James et al., 1989). Sedimentation of the shallow marine carbonates started during the Middle to Late Cambrian consisting of high-energy carbonate facies of the Port-au-Port Group, which occurred during the Early to earliest Middle Ordovician transitioning into low-energy carbonate sediments of the St. George Group (cf. Knight et al., 2008). Taconic fore-arc forcing resulted in distal lithospheric upwarping and rapid sweeping of a tectonic peripheral bulge on the margin, which led to compression, block faulting, uplift, and erosion of the St. George carbonate platform and development of the regional St. George Unconformity (Fig. 2, Mussman and Read, 1986; Knight et al., 2008). A subsequent, tectonically-driven local sea-level rise accommodated deposition of the superjacent deepening-upward carbonates of the Table Head Group (Stenzel et al., 1990; Knight et al., 2008).

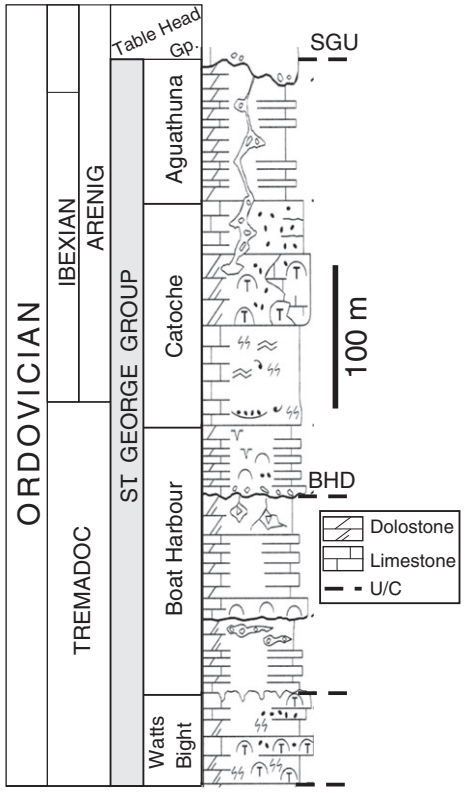

Fig. 2. Stratigraphic framework of the St. George Group and its four formations. The succession shows further the St. George Group Unconformity (SGU), the Boat Harbour Disconformity (BHD) and two unconformities of regional extent (Knight et al., 2008).

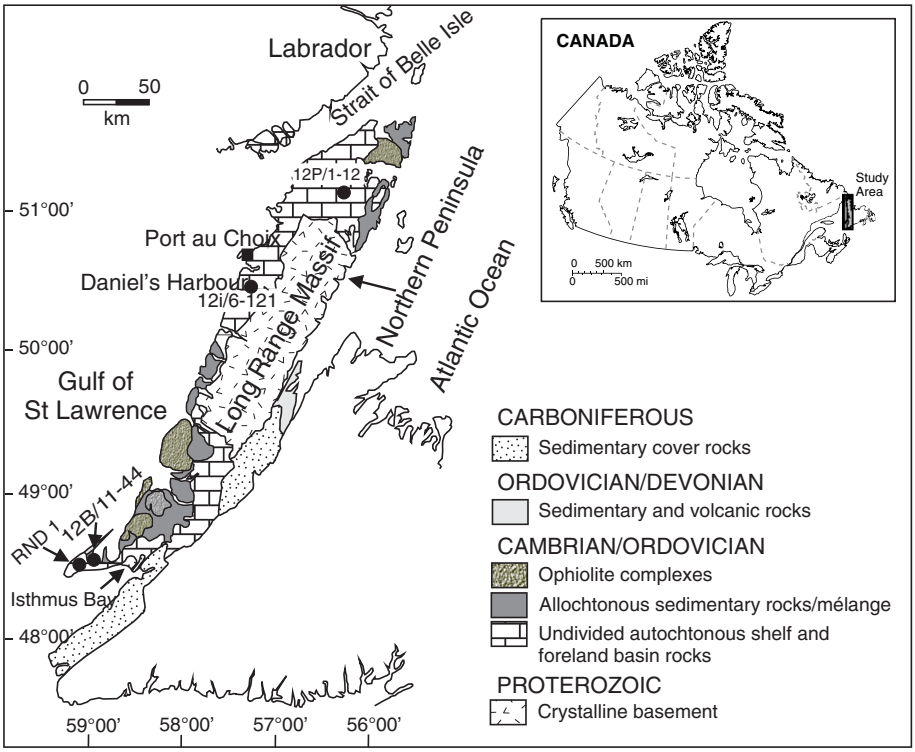

Fig. 1. Map of the study area showing locations of sampled outcrops and cores (Appendix 1), which represent the St. George Group carbonates in western Newfoundland, Canada (adapted from Zhang and Barnes, 2004; Knight et al., in press).

Lithostratigraphy of the St. George Group has been discussed in detail and refined by a number of studies (e.g., Pratt and James, 1986; Knight and James, 1987; Baker and Knight, 1993; Knight et al., 2008). The lithostratigraphic framework (Fig. 2) is briefly summarized here, and from bottom to top it includes the Watts Bight, Boat Harbour, Catoche, and Aguathuna formations (Fig. 2). The upper boundary of the St. George Group (Aguathuna/Table Point formational contact) is marked by the major regional St. George Group Unconformity (SGU; Fig. 2). The St. George Group can be divided into two sedimentary megacycles separated by the Boat Harbour Disconformity (BHD, Fig. 2). Each megacycle is characterized by a large-scale transgressive–regressive succession that resulted in stacking of lower peritidal, middle subtidal and upper peritidal units (Knight and James, 1987; Knight et al., 2008). Multiple stages of dolomitization affected the St. George Group carbonates and are the focus of this study.

3. Methodology

3.1. Sampling and microthermometry

Samples were collected from outcrops and cores at different locations of the Northern Peninsula (Fig. 1) in western Newfoundland from the Watts Bight, Boat Harbour, Catoche, and Aguathuna Formations of the St. George Group (Fig. 2). Modern dolomite-bearing sediments (Ds) protodolomite bearing sabkha sediments were also sampled from the sabkha environments of Abu Dhabi (UAE) and studied for comparison with the dolomites of the St. George Group. X-ray analyses indicate that the sabkha sediment Ds consists of an admixture of 10% dolomite, 22 to 32% calcite, 47 to 55% anhydrite, 10% halite, and 3 to 10% quartz.

Thin sections were stained with Alizarin Red-S and potassium ferricyanide solutions (Dickson, 1966), and examined under a standard polarizing microscope and by cathodoluminoscope (CL). Cathodoluminescence was performed using a ELM-3R cold cathode luminescope operated at about 12 kV accelerating voltage and 0.7 mA gun current intensity. A polished mirror-image slab of each thin section, washed with deionized water, was microsampled by low-speed microdrill.

Microthermometric fluid-inclusion analyses were performed on doubly polished wafers (~100 μm thick) using a Linkam THMSG600 heating-freezing stage. Calibration was achieved with synthetic H_2O and CO_2 fluid inclusion standards that yielded precision of ±0.2 °C at 56.6 °C and ±1 °C at 300 °C. The initial melting temperatures (T_i), last ice melting ($T_{m(ice)}$) and the homogenization temperature (T_h) were measured in primary two-phase (liquid + vapor) inclusions following procedures outlined by Shepherd et al. (1985). Aqueous fluid salinities were calculated using T_m (ice) and the equation of Bodnar (2003).

3.2. Mg-isotope analyses

Subsets of samples were analyzed for Mg isotopes in the labs of the Geological Survey of Canada and Yale University. In the first instance, carbonate powder samples were purified following the protocol described by Wombacher et al. (2009), involving two elutions on 1 mL of AG50W X8 resin. Two elutions were performed because carbonate samples contain high levels of Ca, which is known to cause a matrix effect on Mg isotope ratios (Galy et al., 2001). This approach allows separation of most of the Ca from Mg in the first elution, ensuring good separation of Mg from any residual Ca during the second elution.

Care was taken to verify that the protocol was suitable for all types of samples involved in this study by analyzing synthetic solutions containing major elements (Ca, K, Mg, Fe, Al, Ti) in the range of concentrations observed in the samples, followed by ICP-OES analysis of the recovered fraction to ensure that 100% recovery of Mg was achieved and that it was free of other elements. An aliquot of DSM3 Mg isotope reference standard (Galy et al., 2003) was passed through the resin to verify that the chromatography protocol did not induce fractionation of Mg.

Total milli-equivalent grams per mL was calculated from the elemental analysis, and the determined volume of sample containing 0.48 milli-equivalent grams, representing 40% of maximum resin capacity, was reduced to dryness; then picked up in 1 mL of 10 M HCl to achieve a solution suitable for chromatography. Depending on sample composition, between 10 and 250 μg of Mg was purified. Column blanks were prepared by processing 1 mL of ultrapure 10 M HCl.

Samples, reference materials, and the reference calibration standard (DSM3) were diluted in 0.12 M HCl to obtain a minimum signal of 4 V for ^{24} Mg, but not more than 7 V. The concentration was typically 75 ppb Mg. Once the ^{24} Mg signal intensity for DSM3 was established on any day, samples were diluted to match the signal with 10% tolerance.

Magnesium isotope ratios of samples, blanks, and reference materials were determined on a Nu Plasma double-focusing MC-ICP-MS. The instrument is equipped with twelve fixed faraday detectors and three ion counters. Faraday cups were L5, Axial and H6 for ^{24}Mg, ^{25}Mg and ^{26}Mg respectively, with a mass separation of 0.125 amu. The RF power was 1300 W, plasma gas (coolant) flow 13 L/min, and auxiliary gas 0.9 L/min. A desolvating nebulization system (DNS) was used for sample introduction, with a 'micromist' nebulizer operating at 100 μL/min flow rate. The use of the DNS, in conjunction with diluting with HCl rather than HNO_3, reduced the $^{12}C^{14}N$ interference on ^{26}Mg to insignificant levels, and no action was needed beyond measuring on-peak zero. It was found that the ^{12}C dimer interference on ^{24}Mg could also be kept to insignificant levels by cleaning the sampler cone daily.

Analyses were performed using the sample-standard-bracketing (SSB) technique and on-mass zero measurements. Zero measurements were performed with an integration time of 30 s after rinsing the instrument with 0.12 M HCl for at least 10 min. Samples were analyzed by acquiring 40 measurements with 5 s integration, taken after a 30 s stabilizing time and a 2 min rinse between samples. The Mg-isotope reference material, DSM3, was used in the SSB protocol to account for mass bias drift and heterogeneity problems (cf. Galy et al., 2003).

Each sample, blank and SRM (standard reference material) were analyzed in triplicate by alternating between DSM3 (4 analyses) and sample (3 analyses), starting and finishing with DSM3. Results were accepted only when, 1) the signal intensity of ^{24}Mg for samples and standard were within 10%, 2) both $^{25}Mg/^{24}Mg$ and $^{26}Mg/^{24}Mg$ showed no more than 0.25‰ drift from the first to the last of a group of 4 bracketing DSM3 analyses, and 3) the $\delta^{25}Mg_{DSM3}$ and $\delta^{26}Mg_{DSM3}$ of the three sample replicates fell within 0.1‰, where:

$$\delta^{2X}Mg_{DSM3} = \left(^{2X}Mg/^{24}Mg_{sample} - {}^{2X}Mg/^{24}Mg_{DSM3}\right) / \left(^{2X}Mg/^{24}Mg_{DSM3}\right) \times 1000.$$

Repeated measurements of DSM3 were used to determine the precision of the isotope measurements. Short-term reproducibility determined from 12 measurements was 0.04‰ for δ^{25}Mg and 0.05‰ for δ^{26}Mg. Long-term reproducibility (2σ) determined from 240 analyses of DSM3 over a period of one year was 0.11‰ for δ^{25}Mg and 0.18‰ for δ^{26}Mg. Digestion replicates and column replicates were analyzed to monitor overall uncertainty and uncertainty related to the chemical separation process. The DSM3 processed with this column separation procedure showed that it induced a bias of <0.04‰ on δ^{26}Mg and <0.002‰ on δ^{25}Mg, which is well within uncertainty of the method.

Method blanks were prepared along with the samples in order to determine their impact on the isotope measurements. The blanks

contained no more than 50 ng of Mg, which is <0.5% of the lowest amount of Mg loaded on the column. The impact of blanks on the isotope measurements with <0.05‰ on δ^{26}Mg and <0.02‰ on δ^{25}Mg is well within acceptable limits of the method. The mean δ^{26}Mg values of standards Cambridge 1, JDO-1, and NBS 88a are −2.60 ± 0.08‰, −2.39 ± 0.14‰, and −1.66 ± 0.05‰, respectively.

Another set of samples (marked in bold font in Appendix 1) was analyzed for Mg isotopes in the isotope lab at Yale University following the procedure adopted by Wang et al. (2013). All samples (~100 mg) were sequentially leached with 5 mL of 1 M NH_4Ac, Milli-Q water, 0.1% methanol, Milli-Q water, 0.1% HAc (acetic acid) to remove secondary calcite and surface adsorbed Mg (cf. Liu et al., 2012). During each leaching step, the solution was sonicated for 10 min, followed by centrifuging at 3600 rpm for 10 min. Cleaned samples were finally dissolved in 5 mL 10% HAc, and the supernatants were dried down for column chemistry. Three chromatographic columns were used in this study: 1) an anion column (AG) to remove Fe (also small amounts of Cu and Zn); the samples contain substantial amounts of Fe which could produce a matrix effect, and 2) two cation exchange columns using AG50W-X8 and AG50W-X12 resins to separate Mg from Ca, Sr, and Na. The column chemistry protocol shows that the step-leaching technique efficiently removes calcite and surface adsorbed Mg and reduces the contribution of Mg by silicates.

The isotopic compositions of Sr and Mg, after being separated from the same supernatant, were measured using a Neptune MC-ICP-MS. Both Sr and Mg were picked up in 5% HNO_3 (ρ = 1.020 g/cm^3 at 20 °C). The $^{87}Sr/^{86}Sr$ ratios were corrected for mass bias using $^{88}Sr/^{86}Sr = 8.375209$. Routine measurement of the NBS-987 standard obtained 0.71030 ± 0.00002. Carbonate (contemporary coral) and seawater (*Vineyard Sound seawater*) standards were processed along with leached dolomite solutions (0.70917 ± 0.00002).

Mg-isotope analyses followed the standard-sample bracketing (SSB) technique, and every sample or standard was measured three times. Typical precision is ±0.03 (1σ) errors, and every two samples were bracketed by one of three in-house standards in each experimental run to monitor system drift. Typical overall drift within one session of analysis was <0.1‰, and corrected with the three bracketing standards. Because these variations are much smaller than the heterogeneity of δ^{26}Mg within each lithological group they will not affect our results. Average values of the in-house standards relative to DSM3 are for Yale-1: $\delta^{26}Mg_{DSM3} = -3.54 \pm 0.04‰$ (n = 8), Yale-2: $\delta^{26}Mg_{DSM3} = 0.38 \pm 0.04‰$ (n = 8) and Yale-3: $\delta^{26}Mg_{DSM3} = -5.22 \pm 0.04‰$ (n = 8) and PJA (*Porites* coral from Johnston Atoll): $\delta^{26}Mg_{DSM3} = -1.75 \pm 0.03‰$ (n = 4; cf. Wang et al., 2013). The mean δ^{26}Mg value of the standard Cambridge 1 is −2.58 ± 0.02. The difference in the Δ^{26} Mg values of SRM Cambridge −1 is 0.02‰, which is equivalent to the standard deviation (SD) of the Yale lab and smaller than that of the GSC one. Consequently, this interlaboratory comparison suggests close compatibility in their δ^{26}Mg results despite differences in sample preparation and analytical protocols.

3.3. REE analyses

A subset of sample powder (~10 mg) was digested in 0.075 M pure HNO_3 and analyzed for REEs using a HP 4500*plus* ICP-MS at Memorial University. Relative uncertainties of measurements are better than 3% (cf. Azmy et al., 2011). Normalization of REE concentrations is based on PAAS values (Post-Archean Australian Shale, McLennan, 1989). All geochemical results (isotopes and REEs) are listed in Appendix 1.

The standard deviation of mean values calculated for results from all types of analyses are based on 1σ values.

4. Petrography of dolomites

Petrographic examination of the St. George Group carbonates shows that they range from skeletal grainstones to microbial, fenestral lime mudstones to wackestones (Knight et al., 2008). Dolomitization significantly affected the sediments, which at times, replaced 10s of meters of cyclic shallowing-upward carbonate sediments particularly below disconformities (e.g., Azmy et al., 2008, 2009; Conliffe et al., 2009; Azmy and Conliffe, 2010).

Dolomites of the St. George Group (Fig. 3a–f), from oldest to youngest, are: D1 dolomite (dolomicrite), D2 dolomite (equant, replacive dolomite) and D3 dolomite (large, equant, pore-filling to replacive dolomite). The D1 dolomite (Fig. 3a) consists of dolomicrite and is the most abundant and pervasive of all dolomites (Azmy et al., 2008, 2009); it generally mimics and preserves sedimentary fabrics (e.g., micritic grain size) of its precursor (C1) lime mudstone (Fig. 3b; cf. Sibley, 1982; Budd, 1997). It consists of sub- to euhedral crystals that range from 4 to 50 μm and exhibit dull luminescence under CL (cf. Machel and Mountjoy, 1986, 1990).

D2 dolomite consists of coarse, equant sub- to euhedral crystals that developed during progressive replacement or recrystallization of the host carbonate rock (e.g., Wierzbicki et al., 2006). The crystals vary between ~50 and 150 μm and have cloudy cores with clear rims under plane polarized light (Fig. 3c) and concentrically zoned luminescence (Fig. 3d). Intercrystalline porosity, of up to 10%, in the D2 dolomite was crosscut by solution seams and microstylolites during shallow burial (cf. Azmy et al., 2008, 2009; Conliffe et al., 2009; Azmy and Conliffe, 2010; Azomani et al., 2013).

D3 dolomite consists of pore- and fracture-filling to occasionally replacive sub- to anhedral coarse crystals (>0.5 mm) with a distinctive milky appearance in polished thin sections and slabs. These crystals exhibit undulose extinction and dull luminescence (Fig. 3e–f), which are common features of saddle dolomite (e.g., Azmy et al., 2001; Al-Aasm, 2003; Al-Aasm and Clarke, 2004). D3 saddle dolomite is followed by pore- and fracture-filling C3 calcite (Fig. 3e–f) consisting of coarse crystals (>2 mm) with dull luminescence.

Microthermometric analysis of some St. George Group carbonates (Table 1) indicate that the homogenization temperatures (T_h, average minimum estimate of entrapment temperature) of the primary two-phase fluid inclusions are 112 ± 19 °C and 153 ± 30 °C in the D2 and D3 dolomites, respectively (Table 1, Azmy et al., 2008, 2009). Fluid inclusions within D1 crystals (mainly dolomicrite) were too small to measure. Also, primary fluid inclusions of calcite C3 yielded a T_h value of 90 °C (Table 1). Furthermore, our investigations indicate that average salinities, calculated from the inclusion melting points (T_m) of late phases were between 15 and 25% (Azmy et al., 2008, 2009).

5. Geochemical results

Geochemical results of the carbonates from the St. George Group are in Appendix 1, and summary statistics are in Tables 1 and 2. The lime mudstones (C1) have significantly different δ^{26}Mg values relative to those of the dolomite phases (D1, D2 and D3) from the investigated St. George Group carbonate suite (Table 2). This is true for the dolomites formed at relatively low temperatures as well as to those formed at much higher ones (Table 1). Dolomite phases D1, D2 and D3 also exhibit minor positive shifts in their mean δ^{26}Mg values of about +0.17‰ DSM3 with progressive burial and increasing temperature (Table 1), which is contrary to expectation, if there is a temperature control on isotope fractionation. On the other hand, the modern sabkha dolomites (Ds) have the most positive δ^{26} Mg values (Table 1, −1.03 ± 0.03‰ DSM3), which are similar to those of modern rainwater and seawater of −0.80 ± 0.03‰ DSM3 and −0.81 ± 0.02‰ DSM3, respectively (Hippler et al., 2009; Wombacher et al., 2009; Tipper et al., 2010). However,

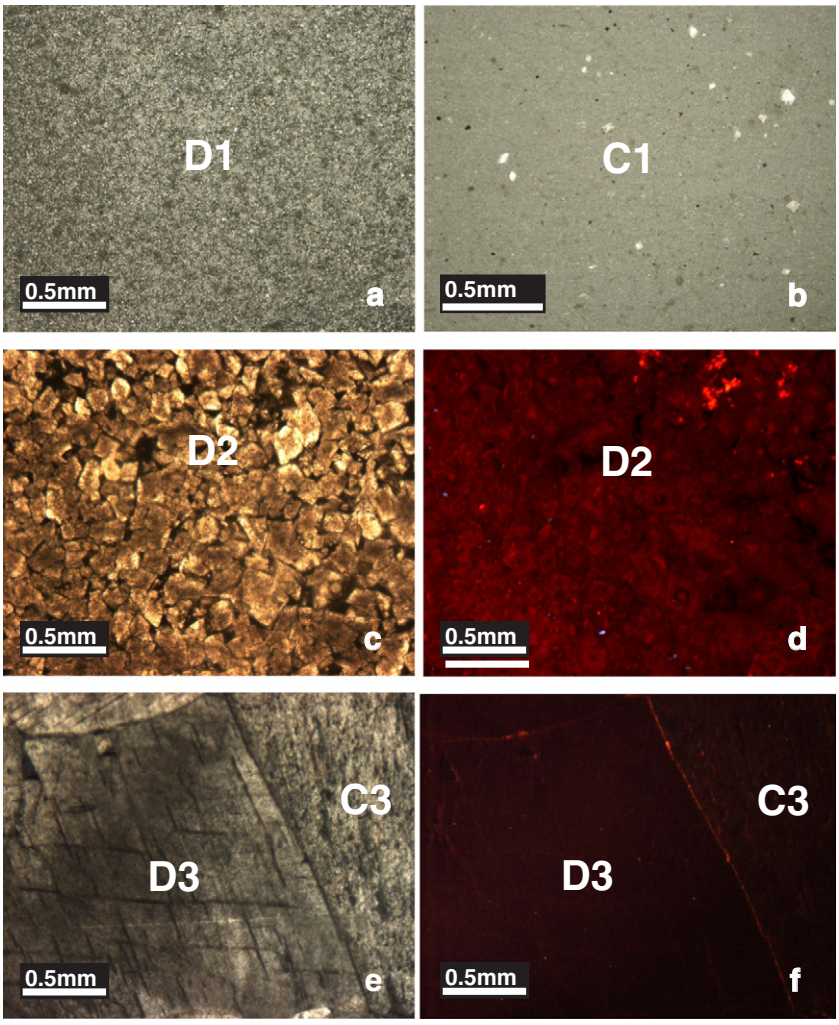

Fig. 3. Photomicrographs of the petrographic characteristics of the St. George Group carbonates, (a) D1 dolomicrite (plane polarized light; Sample R1-130), (b) C1 lime mudstone (plane polarized light; Sample R1-112), (c) D2 dolomite showing cloudy cores and clear rims (plane polarized; Sample BHA13), (d) zoned cathode luminescence of D2 dolomite depicted in (c), (e) C3 calcite postdating D3 saddle dolomite with typical undulose extinction (crossed nichols; Sample BH34), and (f) dull luminescence (cathode) of both C3 calcite and D3 dolomite (e).

caution is needed for the δ^{26}Mg value of the sabkha sediment, which is related to its complex mineralogical mixture, and thus its values may not be singularly reflective of its dolomite content. This would complicate comparisons with other dolomites representing a single mineralogical phase. It is not surprising to note significant differences between the sabkha sediment and the other dolomites including the D1 dolomicrite (Table 2). Another interesting feature is that no significant difference exists in δ^{26}Mg values between the D1 (dolomicrite) and D2 dolomites (Table 2). This observation speaks clearly to and supports the petrographic and chemical observations that the D1 phase was the most likely precursor for the D2 dolomites of the group (cf. Azmy et al., 2008, 2009).

All dolomites have δ^{26}Mg values (Table 1) more positive relative to the latest fracture-filling calcite with -3.20 ± 1.22‰ DSM3. Despite diagenetic alteration of the micritic C1 (lime mudstone) and D1 (dolomicrite), some of their $^{87}Sr/^{86}Sr$ values are similar to those documented for best-preserved Lower to Middle Ordovician marine carbonates of 0.7086 to 0.7092 (Veizer et al., 1999; Shields et al., 2003; Shields and Veizer, 2004; Hanningan et al., 2010; Munnecke et al., 2010).

The D1 dolomicrites and their potential precursor lime mudstones (C1) as well as the replacive mid-burial hydrothermal dolomite (D2) have comparable mean values of total REE ($\sum$REE contents of 12.5 ± 6.1 ppm, 9.7 ± 6.1 ppm, and 8.8 ± 5.0 ppm, respectively, Table 1). The great similarity in $\sum$REE contents between the D1 and D2 dolomites supports their close association already suggested by their Mg isotope values. However, modern sabkha sediments (Ds) and the later-burial fracture-filling dolomite (D3) and calcite (C3) have significantly higher $\sum$REE contents of 19.0 ± 1.0 ppm, 18.8 ± 15.0 ppm and 26.3 ± 17.7 ppm, respectively (Table 1; e.g., Azmy et al., 2011, 2012; Azomani et al., 2013).

6. Discussion

6.1. Mg isotopes — limestones

Limestones, in ascending order, of the Boat Harbour, Catoche and Aguathuna Formations are generally fine-grained lime mudstones (C1) that make their mineralogical assessment difficult. However, the evaluation and comparison of their δ^{26}Mg values with those of other modern carbonates suggests that their values bear no association with those of low-Mg calcite brachiopods, high-Mg calcite echinoids and aragonitic corals (Table 2; Figs. 4 and 5). In contrast, no significant difference was observed between the fine-grained lime mudstones of the St. George Group and those of modern algae, coralline algae and sponges (Table 2).

The mean δ^{26}Mg of -3.35‰ of the Lower Ordovician St. George Group lime mudstones (Table 2) is similar to that of modern algal high-Mg calcite (HMC, >11 mol% $MgCO_3$; Brand and Veizer, 1980) with -3.22‰ but different from that of coral aragonite with -1.78‰

Table 1
Summary statistics of Mg- and Sr-isotope compositions of the Lower Ordovician carbonate phases from the St. George Group in western Newfoundland, Ordovician brachiopods and modern sabkha sediments. The REE data of well-preserved Ordovician brachiopods (bLMC) are from Azomani et al. (2013). Details in text and Appendix 1.

Phase		δ^{26}Mg DSM3‰	δ^{25}Mg DSM3‰	$^{87}Sr/^{86}Sr$	T_h °C	Sr (ppm)	La (ppm)	Ce (ppm)	Pr (ppm)	Nd (ppm)	Sm (PPb)	Eu (ppm)	Gd (ppm)	Tb (ppm)	Dy (ppm)	Ho (ppm)	Er (ppm)	Tm (ppm)	Yb (ppm)	Lu (ppm)	**ΣREE (ppm)**
bLMC	*n*						4	4	4	4	4	4	4	4	4	4	4	3	4	2	4
	Mean						0.362	0.812	0.100	0.373	0.057	0.014	0.061	0.005	0.027	0.005	0.016	0.002	0.015	0.002	1.8
	stdev						0.151	0.256	0.034	0.135	0.020	0.006	0.027	0.003	0.009	0.002	0.009	0.003	0.010	0.002	0.6
	Max						0.545	1.025	0.138	0.557	0.085	0.019	0.098	0.009	0.039	0.008	0.027	0.005	0.025	0.004	2.5
	Min						0.202	0.506	0.063	0.234	0.042	0.007	0.038	0.003	0.019	0.003	0.008	0.000	0.004	0.001	1.2
C1	*n*	5	5	5			23	23	23	23	23	23	23	23	23	23	23	23	23	23	23
	Mean	−3.35	−1.73	0.709134	25		2.202	4.067	0.479	1.720	0.295	0.065	0.323	0.040	0.212	0.041	0.122	0.015	0.104	0.015	9.7
	stdev	0.32	0.19	0.000061	0		1.333	2.854	0.312	1.050	0.165	0.036	0.186	0.022	0.106	0.021	0.064	0.009	0.053	0.008	6.1
	Max	−2.85	−1.44	0.709230	25		5.747	11.773	1.236	4.457	0.725	0.168	0.913	0.107	0.536	0.103	0.323	0.042	0.254	0.038	26.4
	Min	−3.69	−1.95	0.709090	25		0.816	1.233	0.148	0.544	0.084	0.018	0.110	0.009	0.044	0.009	0.029	0.003	0.024	0.002	3.2
C3	*n*	3	3	3	1		12	12	12	12	12	12	12	12	12	12	12	12	12	12	12
	Mean	−3.76	−1.94	0.709147	90		7.036	11.609	1.222	4.265	0.606	0.134	0.699	0.073	0.300	0.053	0.155	0.018	0.125	0.023	26.3
	stdev	0.57	0.27	0.000696			5.556	8.130	0.783	2.625	0.380	0.075	0.432	0.046	0.205	0.036	0.091	0.010	0.062	0.013	17.7
	Max	−3.13	−1.64	0.709930			20.436	28.011	2.658	9.135	1.240	0.275	1.427	0.174	0.774	0.140	0.360	0.041	0.236	0.035	61.0
	min	−4.24	−2.17	0.708600			1.214	3.003	0.379	1.432	0.167	0.050	0.228	0.020	0.006	0.008	0.033	0.008	0.047	0.001	7.0
Ds	*n*	3	3	3		3	3	3	3	3	3	3	3	3	3	3	3	3	3	3	3
	Mean	−1.03	−0.52	0.709133	28	3798	3.735	7.024	0.980	3.920	0.712	0.200	0.796	0.129	0.700	0.131	0.372	0.037	0.255	0.034	19.0
	stdev	0.03	0.02	0.000025	0	203	0.057	0.439	0.013	0.318	0.129	0.013	0.036	0.010	0.099	0.009	0.077	0.017	0.085	0.029	1.0
	Max	−0.99	−0.51	0.709160	28	3979	3.788	7.396	0.994	4.197	0.857	0.215	0.838	0.139	0.775	0.140	0.459	0.048	0.306	0.056	19.9
	Min	−1.05	−0.54	0.709110	28	3579	3.674	6.540	0.969	3.573	0.608	0.190	0.772	0.120	0.588	0.123	0.314	0.017	0.157	0.001	17.9
D1	*n*	9	9	8	9	21	19	19	19	19	19	19	19	19	19	19	19	19	19	19	19
	Mean	−1.92	−1.00	0.709387	35	67	2.587	5.212	0.629	2.388	0.410	0.090	0.443	0.058	0.301	0.055	0.176	0.019	0.139	0.021	12.5
	stdev	0.30	0.16	0.000433	0	44	1.227	2.667	0.312	1.190	0.230	0.041	0.195	0.027	0.120	0.022	0.072	0.011	0.053	0.009	6.1
	Max	−1.30	−0.68	0.710235	35	198	4.859	10.444	1.259	5.012	0.843	0.164	0.836	0.099	0.524	0.102	0.304	0.038	0.250	0.038	24.6
	Min	−2.27	−1.19	0.709080	35	26	1.191	2.258	0.260	0.903	−0.036	0.039	0.117	0.017	0.124	0.020	0.081	−0.006	0.058	0.003	5.1
D2	*n*	13	13	13	7		62	62	62	62	62	62	62	62	62	62	62	62	62	62	62
	Mean	−1.75	−0.90	0.709513	112		1.912	3.592	0.431	1.622	0.291	0.062	0.302	0.043	0.224	0.041	0.125	0.015	0.113	0.016	8.8
	stdev	0.34	0.17	0.000514	19		1.083	2.169	0.263	0.954	0.161	0.033	0.160	0.021	0.113	0.023	0.067	0.009	0.054	0.010	5.0
	Max	−1.06	−0.55	0.710959	125		5.195	9.651	1.208	4.287	0.648	0.127	0.750	0.102	0.522	0.102	0.301	0.035	0.254	0.057	22.2
	Min	−2.17	−1.11	0.709065	73		0.597	1.081	0.110	0.414	0.073	0.013	0.066	0.012	0.059	0.009	0.027	−0.007	0.020	0.001	2.6
D3	*n*	10	10	9	5		15	15	15	15	15	15	15	15	15	15	15	15	15	15	15
	Mean	−1.58	−0.80	0.710156	153		3.596	8.186	1.017	3.769	0.651	0.146	0.631	0.077	0.349	0.060	0.177	0.022	0.135	0.022	18.8
	stdev	0.31	0.16	0.001788	30		2.497	6.886	0.898	3.314	0.529	0.097	0.481	0.052	0.199	0.033	0.090	0.011	0.061	0.009	15.0
	Max	−1.00	−0.51	0.713643	180		10.269	26.917	3.491	12.991	2.049	0.344	1.909	0.210	0.775	0.129	0.357	0.048	0.261	0.037	59.7
	Min	−2.02	−1.05	0.708990	120		1.276	2.476	0.307	1.113	0.202	0.049	0.202	0.033	0.166	0.025	0.073	0.007	0.042	0.008	6.0

Table 2
ANOVA statistics of δ^{26}Mg compositions of various modern biologic carbonates and carbonate components from the Ordovician St. George Group (SGG) and modern dolomites from Abu Dhabi. The modern brachiopods were selected to represent original LMC (low-Mg calcite), the echinoids for HMC (high-Mg calcite), corals for ARAG (aragonite), and the modern algae, coralline algae and sponges for another variety of HMC.

Component	*N*	Mean	SD	*p*	Source data
C1–lime mudstone (SGG)	5	−3.35	0.32		This study
Modern brachiopods (LMC)	6	−2.08	0.15	0.0001	Hippler et al. (2009) and Wombacher et al. (2011)
Modern echinoids (HMC)	11	−2.56	0.11	0.0001	Hippler et al. (2009)
Modern corals (ARAG)	11	−1.78	0.16	0.0001	Hippler et al. (2009) and Wombacher et al. (2011)
Modern algae, coralline algae & sponges (HMC)	17	−3.22	0.13	0.165	Hippler et al. (2009) and Wombacher et al. (2011)
Sabkha dolomite (Abu Dhabi)	3	−1.03	0.03		This study
D1 dolomite (SGG)	9	−1.92	0.30	0.0001	This study
D2 dolomite (SGG)	13	−1.75	0.33	0.0001	This study
D3 dolomite (SGG)	10	−1.58	0.31	0.0001	This study
C1 lime mudstone–D1 dolomite				0.0001	This study
C1 lime mudstone–D2 dolomite				0.0001	This study
C1 lime mudstone–D3 dolomite				0.0001	This study
D1 dolomite–D2 dolomite				0.224	This study
D2 dolomite–D3 dolomite				0.238	This study

Note: Sabkha dolomite Mg-isotope values may be a reflection of their mixed mineralogy (section 4).

and of brachiopod low-Mg calcite (LMC, <4 mol% $MgCO_3$; Brand and Veizer, 1980) with −2.08‰ (Galy et al., 2002; Tipper et al., 2006a, b; Immenhauser et al., 2010). This association suggests that algae were the most likely source for the lime mud of the St. George Group, and further, this source material consisted originally of high-Mg calcite. Except for algal lamination, the absence of other biogenic textures provides further support that the lime mud of the St. George carbonates had an algal origin. Diagenesis may drastically shift/alter the trace element and isotopic compositions (C, O, Sr) of carbonates, controlled in part, by the openness of the system and the chemical composition of the reacting fluids (cf. Brand and Veizer, 1980, 1981; Veizer, 1983; Banner and Hanson, 1990; Brand et al., 2010). The similarity in Mg isotope values between the St. George lime mudstones and the modern algal HMC, since the former are now consisting of diagenetic low-Mg calcites, suggests that diagenetic stabilization of the HMC sediments to LMC did not bring about a significant change in Mg isotope values. This is not completely unexpected since the isotopic compositions of modern seawater and meteoric waters (rain, ground and surface) are similar (Figs. 4 and 5; e.g., Galy et al., 2002; Wombacher et al., 2009; Immenhauser et al., 2010; Tipper et al., 2010), and exposure to or interaction with them during diagenesis may shift the elemental Mg contents (cf. Veizer, 1983; Brand, 1990) but apparently not their Mg isotope compositions.

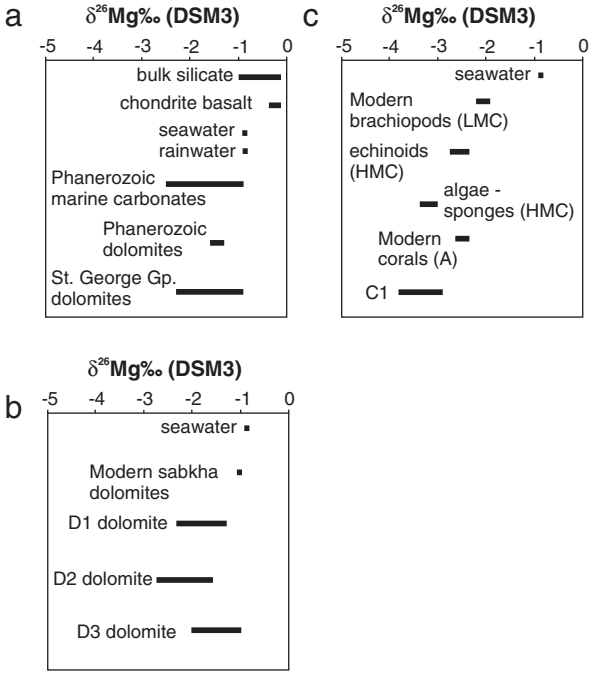

Fig. 4. Bar chart summary ranges of δ^{26}Mg compositions of various lithologies and seawater. a, Includes seawater & rain water, bulk silicates (Teng et al., 2010), chondrites/basalts (Teng et al., 2010; Pogge von Strandmann et al., 2011), Phanerozoic marine carbonates (Galy et al., 2002; Tipper et al., 2006a, b; Immenhauser et al., 2010), Phanerozoic dolomites (Galy et al., 2002; Chang et al., 2003; Young and Galy, 2004; Brenot et al., 2008; Tipper et al., 2008; Wombacher et al., 2009; Jacobson et al., 2010; Pokrovsky et al., 2011), and dolomites of the Lower Ordovician St. George Group (this study). b, Includes seawater and the four dolomites (Ds — modern sabkha dolomite and the D1 to D3 dolomites of the St. George Group). c, Includes modern seawater-^{26}Mg values, and modern brachiopods (LMC — low-Mg calcite), echinoids (HMC — high-Mg calcite), algae–sponges (HMC), corals (A — aragonite), and C1 lime mudstone of the St. George Group.

The Mg-isotope values of the lime mudstones of the St. George Group not only suggest an algal origin for the sediments but also speak to their high-Mg calcite mineralogy (Fig. 4c). Furthermore, the δ^{26}Mg values of the C1 lime mudstones fall along the Mg isotope fractionation line (Fig. 5) of modern carbonates with almost no deviation, and their near-micritic grain size and limited recrystallization suggest that their δ^{26}Mg is likely near-primary (e.g., Mavromatis et al., 2013). Thus, they reflect the Mg-isotope composition of seawater during the Paleozoic or at least during the Ordovician and also support the concept of HMC-dominated seas instead of low-Mg calcite (Stanley, 2008). However, more work is needed to reach more conclusive interpretations regarding this important issue.

6.2. Mg isotopes — dolomites

The details of the Mg-isotope results of the St. George Group carbonates are summarized in Table 1. The slope (0.514) of the linear correlation ($R^2 = 0.99$) between the δ^{26}Mg and δ^{25}Mg signatures of the investigated carbonates (Fig. 6) is consistent with values documented in other studies of different rock and river systems (e.g., Galy et al., 2001; Young and Galy, 2004; Brenot et al., 2008; Immenhauser et al., 2010; Wimpenny et al., 2011; Riechelmann et al., 2012).

6.2.1. Precursor and fluid composition control

Recent Mg isotope studies showed that modern rain and seawater have almost identical δ^{26}Mg signatures (−0.80 ± 0.02‰ DSM3, and −0.81 ± 0.03‰ DSM3, respectively; Hippler et al., 2009; Wombacher et al., 2009; Tipper et al., 2010), which suggests that Mg isotopes do not fractionate during water evaporation. This is also consistent with the Mg isotopic composition of the modern sabkha sediment (Ds), which has comparable mean δ^{26}Mg value (−1.03 ± 0.03‰ DSM3, Table 1) with that of modern seawater. If Mg isotopes fractionate during evaporation, the sabkha sediments should be more enriched in ^{26}Mg than seawater because sabkhas

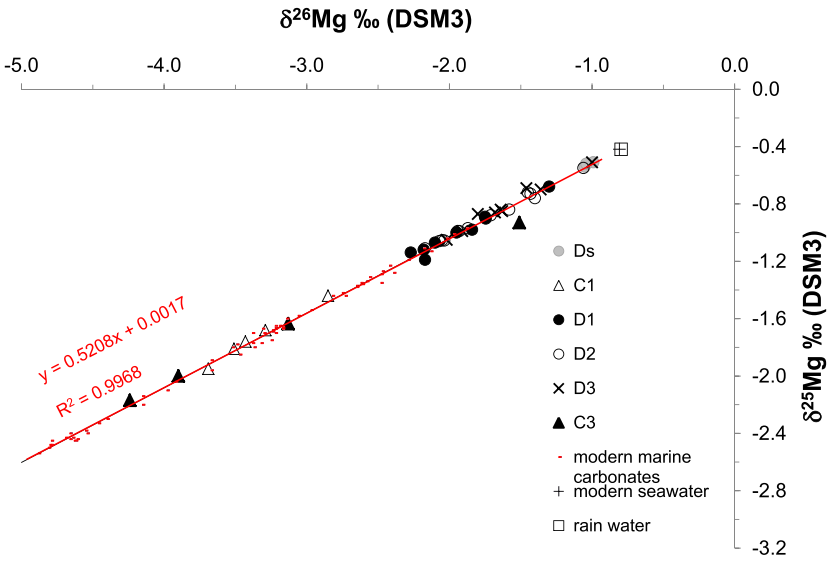

Fig. 5. Correlation of Mg-isotope compositions of carbonates from this study (C1, D1, D2, D3, C3) and counterparts of modern (Ds) and Phanerozoic rocks (red dots) showing scatter diagram of δ^{26}Mg vs. δ^{25}Mg of the investigated dolomite and calcite phases and of modern marine carbonates (Hippler et al., 2009; Tipper et al., 2010; Wombacher et al., 2011). Values were recalculated based on the equation of Galy et al. (2002).

are evaporative environments, but instead they are slightly depleted by 0.22‰. The depletion can be attributed to the primary Mg isotope signature of Persian Gulf seawater, and/or minor contributions from bacterial activity associated with sabkha sediment precipitation (Carder et al., 2004, 2005; Tipper et al., 2006a, b; Bontognali et al., 2012). Otherwise, it agrees with the documented depletion caused by bacteria during precipitation of bacterial dolomite (up to 3.07‰ DSM3; Carder et al., 2005) and with the general depletion and wide variation in the range of δ^{26}Mg signatures of biogenic modern marine carbonates (e.g., Carder et al., 2004, 2005; Eisenhauer et al., 2009; Hippler et al., 2009; Wombacher et al., 2011). These are likely dominated by vital and possibly mineralogical controls rather than temperature of the ambient water (Hippler et al., 2009; Rustad et al., 2010; Schauble, 2011). A vital and/or mineralogical effect may explain the wide range of Mg isotope compositions observed in Phanerozoic lime mudstones (−4.5 to −1‰ DSM3, Galy et al., 2002; Carder et al., 2004, 2005; Tipper et al., 2006a, b; Eisenhauer et al., 2009; Immenhauser et al., 2010; Li et al., 2012; this study) that forms by the disintegration of biogenic carbonates or from precipitates by microbial mediation.

Temperature seems an unlikely control on the fractionation of Mg isotopes during the formation of D1 dolomite (Fig. 3a; cf. Azmy et al., 2008, 2009; Geske et al., 2012). Instead, the early-diagenetic D1 dolomite most likely inherited its chemical (elemental and isotopic) signatures from the precursor carbonates and the diagenetic fluid (s). The near-micritic grain size of the precursor C1 (Fig. 3b) indicates that the lime mudstones were not extensively altered by meteoric water before dolomitization (Brand and Veizer,

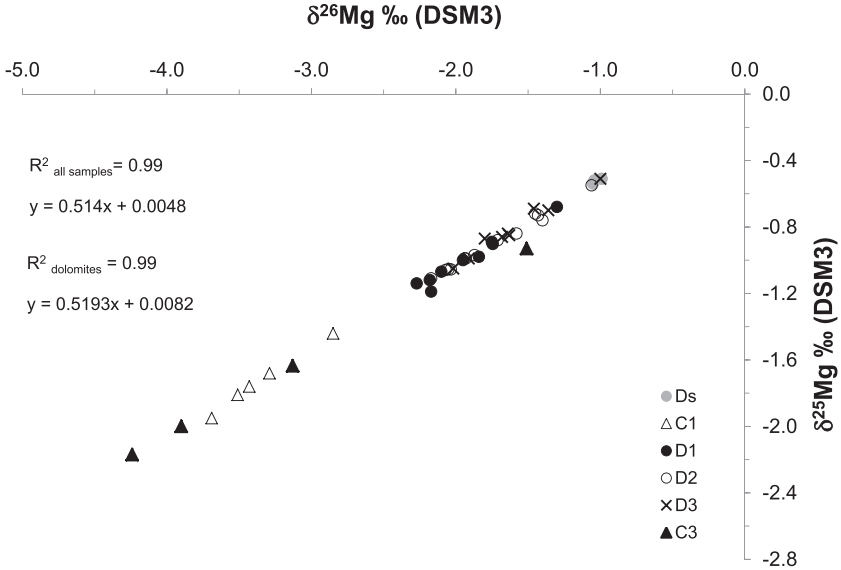

Fig. 6. Scatter diagram of δ^{26}Mg vs. δ^{25}Mg values of St. George Group carbonates. Results include calcites (C1 and C3), dolomites (D1, D2, D3) and modern sabkha sediments (Ds), and regression line values of a) the total samples and b) dolomite populations. Values were recalculated based on the equation of Galy et al. (2002).

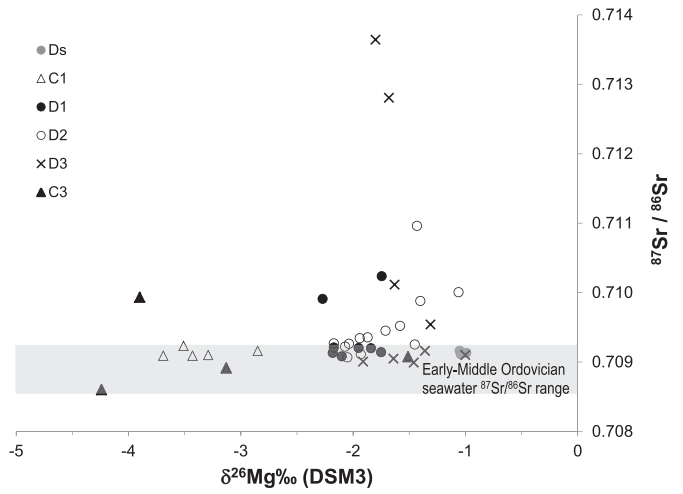

Fig. 7. Scatter diagram of δ^{26}Mg vs. $^{87}Sr/^{86}Sr$ of the St. George Group carbonates. The shaded area represents the range of best preserved (least radiogenic) signatures documented for Early–Middle Ordovician seawater (Shields et al., 2003; Shields and Veizer, 2004; Munnecke et al., 2010). The $^{87}Sr/^{86}Sr$ data are compiled from Azmy et al. (2008, 2009); Conliffe et al. (2010), and Azmy and Conliffe (2010).

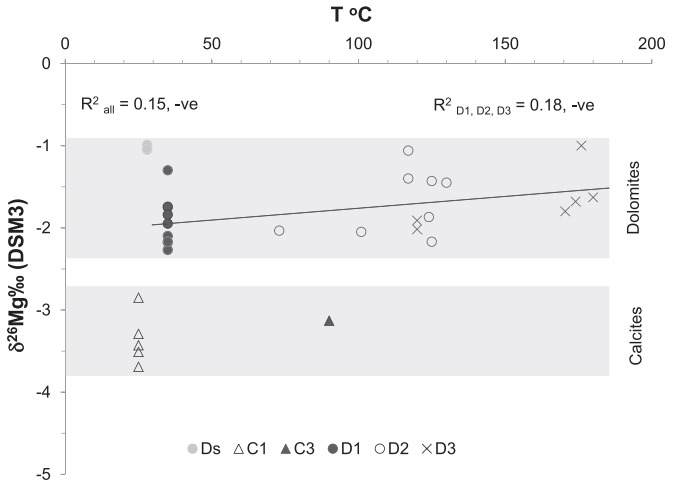

Fig. 8. Scatter diagram of δ^{26}Mg and temperatures of modern sabkha sediment and Lower Ordovician carbonates. Shaded areas represent the general calcite and dolomite trends. The calcites and dolomites show no significant correlation between Mg-isotope compositions and formational temperatures.

1980; Budd, 1997), which also supports preservation of their near-primary Mg isotope compositions.

The δ^{26}Mg values of the D1 dolomites are depleted compared with values of modern marine and meteoric waters (Fig. 4) and they span a wider range than that documented for some other Phanerozoic dolomites (Fig. 4, Tipper et al., 2006b, 2008). The range of δ^{26}Mg values of modern biogenic carbonates (−5.57 to −1.52‰ DSM3, Hippler et al., 2009; Wombacher et al., 2009) bracket those of the Lower Ordovician St. George lime mudstones (C1, −3.69 to −2.85‰ DSM, Table 1 and Figs. 4 and 5) and thus suggesting that the difference between the δ^{26}Mg value of Ordovician seawater and our present day counterpart was comparable rather than dramatic. This is also consistent with the range of δ^{26}Mg values of the D1 dolomite (Table 1), which is bracketed by those of the meteoric/marine waters and the counterparts of their precursor Lower Ordovician St. George Group C1 lime mudstones and modern calcites (Fig. 5). Hence, suggesting formation from a mixture of marine and meteoric waters dolomitizing fluid.

Petrographic and geochemical studies of the St. George Group dolomites (e.g., Azmy et al., 2008, 2009; Conliffe et al., 2009) suggest that the fabric-retentive and near-micritic D1 dolomite, along with its low Sr contents (67 ± 44 ppm compared with 3798 ± 203 ppm in Ds modern sabkha, Table 1) are characteristic of non-evaporative dolomite (e.g., Budd, 1997; Azmy et al., 2008, 2009; Conliffe et al., 2009) and consistent with formation from mixed waters (marine and meteoric) during an early diagenetic stage under near-surface conditions. Oxygen- and Sr-isotope studies on the same rocks (e.g., Azmy et al., 2008, 2009) indicated that the estimated oxygen-isotopic composition of the fluid that precipitated D1 fits between the estimated δ^{18}O values of Ordovician meteoric and seawaters, and some of the $^{87}Sr/^{86}Sr$ signatures of D1 are similar to their precursor C1 and still fall within the range documented for Early Ordovician seawater (Fig. 7). In addition, the enriched δ^{18}O signature documented for D1 was −2.9‰ (VPDB), and previous studies indicate that dolomitization leads to enrichment in δ^{18}O by 2 to 4‰ or more (e.g., Land, 1983). Application of the $\Delta_{dolomite-calcite}$ enrichment to the most positive δ^{18}O value from the St. George dolomite will reduce it to ~−7‰ (VPDB), which is within the range (−6 to −10‰, VPDB) documented for the best preserved carbonates precipitated from Early Ordovician seawater (Veizer et al., 1999). Therefore, it is very unlikely that D1 dolomite had a sabkha origin particularly with the lack of co-occurrence of evaporites and Mg-isotope agreement (Table 2). Instead, the Mg-isotopic signatures of the D1 dolomite support the concept of mixed-water and near-surface dolomitization.

6.2.2. Temperature control

Our suite of samples includes modern sabkha sediment (Ds), lime mudstones (C1) and dolomicrites (D1) as well as deep burial carbonates (D2, D3 and C3). The modern sabkha sediment probably precipitated at about 28 °C (mean annual air temperature of the sampling area in Abu Dhabi, UAE), whereas the micritic C1 (Azmy et al., 2008, 2009) precipitated in a warm, tropical shallow-shelf environment of about 25 °C. The near-micritic grain size of the D1 dolomite suggests deposition at a near-surface temperature of ~35 °C (cf. Azmy et al., 2008, 2009; Conliffe et al., 2009, 2010).

Fractionation of isotopes, particularly those of non-metals, is well known to decrease with increasing temperature (Faure and Mensing, 2005), but the Mg-isotope compositions of the St. George Group dolomites show an opposite, and poorly-defined or no trend (Fig. 8, Table 1; e.g., Geske et al., 2012). Microthermometric analyses of the D2 and D3 dolomites and C3 calcite indicate precipitation at higher temperatures consistent with deep burial settings (Table 1). Moreover, the δ^{26}Mg signatures of investigated dolomites exhibit insignificant negative correlation with temperatures of precipitation (Fig. 8). The mid- and late burial D2 and D3 dolomites of higher temperature diagenetic settings have slightly more positive δ^{26}Mg signatures compared with those of the near-surface D1 dolomite, coupled with no significant trends between the D1–D2 and D2–D3 types (Tables 1, 2; Azmy et al., 2008, 2009; Conliffe et al., 2009). It is unlikely that the δ^{26}Mg of the dolomitizing fluid was increasingly enriched with progressive burial to overprint the effect of thermal fractionation unless the thermal fractionation of Mg isotopes is insignificant and/or smaller than the analytical uncertainty. Therefore, temperature is an unlikely influencing factor on the Mg-isotopic compositions of the dolomites. Instead, the crustal rocks, such as the ^{26}Mg-rich siliciclastics (e.g., sandstones, Fig. 4), through which the basinal fluids circulated under semi-closed system conditions (Azmy et al., 2008, 2009; Conliffe et al., 2009, 2012; Azomani et al., 2013) were the cause for the enrichment in ^{26}Mg of the St. George dolomitizing fluids and hence of the burial D2 and D3 dolomite δ^{26}Mg values. On the other hand, earlier experimental studies (e.g., Mavromatis et al., 2013) on Mg-isotope fractionation in calcites indicated a negative correlation between growth rate and isotope fractionation. However, results of those studies apply

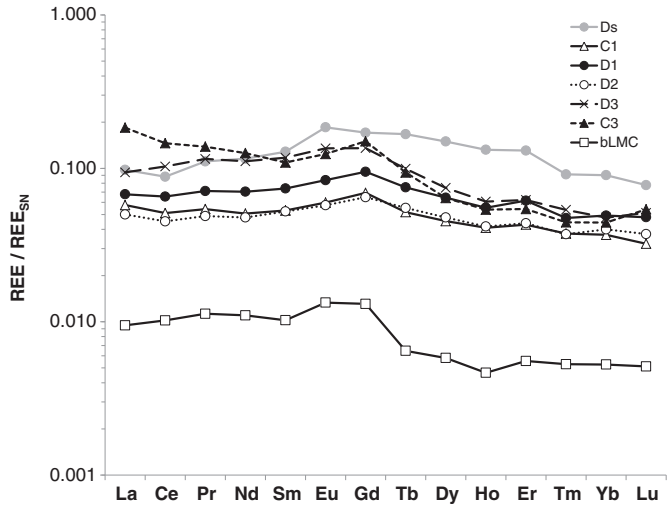

Fig. 9. Mean REE concentrations (REE_{SN}) shale-normalized (PAAS) values of calcite and dolomite phases from the Lower Ordovician St. George Group and modern sabkha sediments. The REE data of well-preserved Ordovician brachiopods (bLMC — biogenic low-Mg calcite) are from Azomani et al. (2013).

to calcites at surface pressure and temperature, which makes them incompatible with diagenetic dolomites from burial settings.

The highly radiogenic $^{87}Sr/^{86}Sr$ ratios of many of those dolomites (Fig. 7) support the circulation of the diagenetic fluids through clastic crustal rocks. The lack of strong evidence for thermal fractionation of Mg isotopes in the hydrothermal dolomites (D2 and D3) deposited at different temperatures and within the same basin is also consistent with the weak fractionation of Mg isotopes at near-surface temperatures suggested by earlier studies (e.g., Hippler et al., 2009; Immenhauser et al., 2010; Li et al., 2012; Pogge von Strandmann et al., 2011; Wombacher et al., 2011).

Depletion in mean $\delta^{26}Mg$ of the latest fracture/pore filling C3 calcite cement (-3.76 ± 0.57‰ DSM3) relative to those of the related D2 and D3 dolomites (Fig. 6 and Table 1) implies that it precipitated from a different fluid phase that was introduced during the latest stage of diagenesis. This concept is consistent with the conclusions of petrographic and geochemical studies of the same carbonates (e.g., Azmy et al., 2008, 2009; Conliffe et al., 2009).

In summary, there is no support for appreciable thermal fractionation of Mg isotopes in the currently investigated dolomites, instead it is suggested that there was a significant influence of the Mg-isotope composition of the diagenetic fluids on the $\delta^{26}Mg$ values of the diagenetic carbonates. It is conceivable that, for well-constrained diagenetic successions, the $\delta^{26}Mg$ ratio of diagenetic dolomite may provide clues about the source of Mg and hence shed light on the dolomitization process(es).

6.3. Rare earth elements

The REE composition of diagenetic carbonates is controlled by its precursors (e.g., Azmy et al., 2011) and reflected in the retention of their REE normalized pattern (Fig. 9) despite enrichment in their total REE contents ($\sum$REE, Table 1). Therefore, correlation of the REE compositions of dolomites with those of their precursor calcite may shed light on the nature of the dolomitizing fluids. The mean $\sum$REE composition of the precursor C1 (9.7 ± 6.1 ppm, Table 1) is comparable to slightly lower than other altered Paleozoic lime mudstones (Azmy et al., 2011, their Table 1), possibly due to the relative preservation of near-micritic grains and thus limited recrystallization of some samples. However, the $\sum$REE of C1 lime mudstones is higher (at least by a factor of 3) compared to that of modern and well-preserved Paleozoic brachiopod shells, particularly those from the Ordovician, (Fig. 9 and Table 1) of similar warm-water depositional environment (Azmy et al., 2011, 2012; Azomani et al., 2013). This trend is consistent with the increasing enrichment of REEs noted in carbonates with progressive diagenetic alteration (e.g., Shaw and Wasserburg, 1985; Azmy et al., 2011, 2012).

The D1 dolomite has mean $\sum$REEs (12.5 ± 6.1 ppm, Table 1) similar to that of the C1 lime mudstone, which is supported by the petrographic preservation of near-micritic grains and early stage near-surface dolomitization (Azmy et al., 2008, 2009). On the other hand, the mean $\sum$REEs of the D2 dolomite (8.8 ± 5.0 ppm, Table 1) are comparable to those of the D1 dolomite and C1 lime mudstone (Fig. 9). This suggests that the D2 dolomite, a mainly replacive carbonate phase of mid-burial setting, inherited its REE composition from the precursor D1 dolomite. This was ultimately sourced from basinal fluids similar to those involved in the formation of the D1 dolomite that circulated under semi-closed to closed conditions, all supported by petrography and limited enrichment (~0.17‰) in the mean δ^{26} Mg values of the D1–D2 dolomites (Table 2). The latest fracture-filling D3 saddle dolomite has a higher mean $\sum$REE (18.8 ± 15.0 ppm, Table 1) because it is not a replacive phase and most of its REE signature is derived from that of late-source fluids. Similarly, the fracture-filling C3 calcite cement even has a higher mean $\sum$REE (26.3 ± 17.7 ppm, Table 1), thus suggesting that it was emplaced at a later stage and from a different fluid phase. The $\sum$REE of the sabkha Ds (19.0 ± 1.0 ppm, Table 1) is high and comparable to that of D3 dolomite because it reflects the influence of evaporation, which is clear in the higher contents of mid- and heavy REEs and the highest Sr contents (3798 ± 203 ppm, Table 1; Fig. 9).

7. Conclusions

The succession of the St. George Group provided us with an opportunity to study the petrographic and geochemical evolution of five carbonate phases within its four formations, and in particular their Mg-isotopic compositions. The phases identified within the sequence are lime mudstones (C1), early diagenetic dolomicrite (D1), mid-burial hydrothermal dolomite (D2), late-burial saddle dolomite (D3) and late-stage coarse calcite (C3).

The $\delta^{26}Mg$ values of the lime mudstones from the St. George Group bear strong resemblance to $\delta^{26}Mg$ values of modern high-Mg calcite algae. Thus, in conjunction with petrographic and other geochemical evidence, it is proposed that the lime mudstone was sourced from Ordovician algae with precursor high-Mg calcite mineralogy.

The $\delta^{26}Mg$ values of the earliest dolomite phase, D1 dolomicrite, are bracketed by those of modern meteoric and seawater and other Phanerozoic carbonates. This suggests that D1 dolomite likely formed from dolomitizing fluids consisting of a mixture of marine and meteoric waters in a near-surface setting. The similarity in $\delta^{26}Mg$ between D1 and D2 dolomites suggests that the former may have played a major role in the formation of the latter throughout the St. George Group.

Ranges of $\delta^{26}Mg$ values of the late hydrothermal D2 and D3 dolomites and of early D1 dolomite overlap considerably, which implies that the hydrothermal fluids possibly originated from solutions of Mg-isotopic compositions similar to those sourcing the D1 or probably from dolomitizing fluids where their Mg-isotope composition evolved through circulation in the crust during progressive burial of the sediments. The Mg-isotope composition of the precursor carbonate (lime mudstone) for the replacive dolomites (e.g., D1 and D2) may have also contributed with a buffering effect on the $\delta^{26}Mg$ values of those dolomites.

The mean $\delta^{26}Mg$ values of the investigated Lower Ordovician dolomites show only a slightest enrichment with temperature, suggesting that temperature is not the controlling factor of the

δ^{26}Mg signatures of the dolomites. Instead, the Mg-isotopic composition of the diagenetic fluids circulating through ^{26}Mg-rich siliciclastic crustal rocks and possibly other silicates, under closed to semi-closed system conditions, imparted Mg-isotope characteristics on these later formed dolomites and calcites.

Supplementary data to this article can be found online at http://dx.doi.org/10.1016/j.chemgeo.2013.07.015.

Acknowledgment

This project was supported by the Petroleum Research Atlantic Canada (PRAC) and Petroleum Exploration Enhancement Program (PEEP; Karem Azmy), and by Geomapping for Energy and Minerals of the Earth Science Sector, Natural Resources Canada (NRC–20120210), and by Natural Science and Engineering Research Council of Canada (NSERC–7961, Uwe Brand; NSERC–812005, Ihsan Al-Aasm). We thank Chao Liu for technical assistance.

References

Al-Aasm, I., 2003. Origin and characterization of hydrothermal dolomite in the Western Canada Sedimentary Basin. Journal of Geochemical Exploration 78–79, 9–15.
Al-Aasm, I., Clarke, J.D., 2004. The effect of hydrothermal fluid flow on early diagenetic dolomitization: an example from the Devonian Slave Point Formation, northwest Alberta, Canada. American Association of Petroleum Geologists Bulletin Hedberg Series 1, 297–316.
Azmy, K., Conliffe, J., 2010. Dolomitization of the lower St. George Group on the Northern Peninsula in western Newfoundland: implications for lateral distribution of porosity. Bulletin of Canadian Petroleum Geology 58, 1–14.
Azmy, K., Veizer, J., Misi, R., De Olivia, T., Sanches, A.L., Dardenne, M., 2001. Isotope stratigraphy of the neoproterozoic carbonate Vazante Formation Saõ Francisco Basin, Brazil. Precambrian Research 112, 303–329.
Azmy, K., Lavoie, D., Knight, I., Chi, G., 2008. Dolomitization of the Aguathuna carbonates in western Newfoundland, Canada: implications for a potential hydrocarbon reservoir. Canadian Journal of Earth Sciences 45, 795–813.
Azmy, K., Knight, I., Lavoie, D., Chi, G., 2009. Origin of the Boat Harbour dolomites of St. George Group in western Newfoundland, Canada: implications for porosity controls. Bulletin of Canadian Petroleum Geology 57, 1–24.
Azmy, K., Brand, U., Sylvester, P., Gleeson, S., Logan, A., Bitner, M.A., 2011. Biogenic low-Mg calcite (brachiopods): proxy of seawater–REE composition, natural processes and diagenetic alteration. Chemical Geology 280, 180–190.
Azmy, K., Poty, E., Mottequin, B., 2012. Frasnian–Famenian pre-event: a record from the Dinant Basin, Belgium. Palaeogeography, Palaeoclimatology, Palaeoecology 313, 93–106.
Azomani, E., Azmy, K., Blamey, N., Brand, U., Al-Aasm, I., 2013. Origin of Lower Ordovician dolomites in eastern Laurentia: controls on porosity and implications from geochemistry. Marine and Petroleum Geology 40, 99–114.
Baker, D., Knight, I., 1993. The Catoche Dolomite Project, Anticosti Basin, Eastern Canada: CERR Report. Memorial University of Newfoundland, St. John's Newfoundland (174 pp.).
Banner, J.L., Hanson, G.N., 1990. Calculation of simultaneous isotopic and trace element variations during water–rock interaction with applications to carbonate diagenesis. Geochimica et Cosmochimica Acta 54, 3123–3137.
Bodnar, R.J., 2003. Interpretation of data from aqueous–electrolyte fluid inclusions. In: Samson, I., Anderson, A., Marshal, D. (Eds.), Fluid Inclusions: Analyses and Interpretation. Mineralogical Association of Canada. Short Course Series, 32, pp. 81–100.
Bontognali, T.R.R., Vasconcelos, C., Warthmann, R.J., Lundberg, R., McKenzie, J.A., 2012. Dolomite-mediating bacterium isolated from the sabkha of Abu Dhabi (UAE). Terra Nova 24, 248–254.
Brand, U., 1990. Chemical diagenesis and dolomitization of Paleozoic high-Mg calcite crinoids. Carbonates and Evaporites 5, 179–195.
Brand, U., Veizer, J., 1980. Chemical diagenesis of a multicomponent carbonate system: 1, trace elements. Journal of Sedimentary Petrology 50, 1219–1236.
Brand, U., Veizer, J., 1981. Chemical diagenesis of a multicomponent carbonate system: 2, stable isotopes. Journal of Sedimentary Petrology 51, 987–997.
Brand, U., Azmy, K., Tazawa, J.-I., Sano, H., Buhl, D., 2010. Hydrothermal diagenesis of Paleozoic seamount carbonate components. Chemical Geology 278, 173–185.
Brenot, A., Cloquet, C., Vigier, N., Carignan, J., France-Lanord, C., 2008. Magnesium isotope systematics of the lithologically varied Moselle river basin France. Geochimica et Cosmochimica Acta 72, 5070–5089.
Budd, D.A., 1997. Cenozoic dolomites of carbonate islands: their attributes and origin. Earth-Science Reviews 42, 1–47.
Carder, E.A., Galy, A., Elderfield, H., 2004. The magnesium isotopic composition of oceanic water masses. Geochimica et Cosmochimica Acta 68, A329.
Carder, E.A., Galy, A., McKenzie, J.A., Vasconcelos, C., Elderfield, H.E., 2005. Magnesium isotopes in bacterial dolomites: a novel approach to the dolomite problem. Geochimica et Cosmochimica Acta 69 (10), A213.
Chang, V.T.-C., Masishima, A., Belshaw, N.S., O'Nions, R.K., 2003. Purification of Mg from low Mg biogenic carbonates for isotope ratio determination using multi-collector ICP-MS. Journal of Analytical Atomic Spectrometry 18, 296–301.
Conliffe, J., Azmy, K., Knight, I., Lavoie, D., 2009. Dolomitization in the Lower Ordovician Watts Bight Formation of the St Georges Group, western Newfoundland. Canadian Journal of Earth Sciences 46, 247–261.
Conliffe, J., Azmy, K., Gleeson, S.A., Lavoie, D., 2010. Fluids associated with hydrothermal dolomitization in St. George Group, western Newfoundland, Canada. Geofluids 9, 1–16.
Conliffe, J., Azmy, K., Greene, M., 2012. Hydrothermal dolomites in the Lower Ordovician Catoche Formation. Marine and Petroleum Geology 30, 161–173.
de Villiers, S., Dickson, J.A.D., Ellam, R.M., 2005. The composition of the continental river weathering flux deduced from seawater Mg isotopes. Chemical Geology 216, 133–142.
Dickson, J.A.D., 1966. Carbonate identification and genesis as revealed by staining. Journal of Sedimentary Petrology 36, 491–505.
Eisenhauer, A., Kısakürek, B., Böhm, F., 2009. Marine calcification: an alkali metal isotope perspective. Elements 5, 365–368.
Faure, G., Mensing, T.M., 2005. Isotopes: Principles and Applications, third edition. John Willey and Sons, Inc., Hoboken, New Jersey (897 pp.).
Galy, A., Belshaw, N.S., Halicz, L., O'Nions, R.K., 2001. High precision measurement of magnesium isotopes by multiple-collector inductively coupled plasma mass spectrometry. International Journal of Mass Spectrometry 208, 89–98.
Galy, A., Bar-Matthews, M., Halicz, L., O'Nions, R.K., 2002. Mg isotopic composition of carbonate: insight from speleothem formation. Earth and Planetary Science Letters 201, 105–115.
Galy, A., Yoffe, O., Janney, P.E., Williams, R.W., Cloquet, C., Alard, O., Halicz, L., Wadhwa, M., Hutcheon, I.D., Ramon, E., Carignan, J., 2003. Magnesium isotope heterogeneity of the isotopic standard SRM 980 and new reference materials for magnesium isotope-ratio measurements. Journal of Analytical Atomic Spectrometry 18, 1352–1356.
Geske, A., Zorlu, J., Richter, D.K., Buhl, D., Niedermayr, A., Immenhauser, A., 2012. Impact of diagenesis and low grademetamorphosis on isotope (δ^{26}Mg, δ^{13}C, δ^{18}O and ^{87}Sr/^{86}Sr) and elemental (Ca, Mg, Mn, Fe and Sr) signatures of Triassic sabkha dolomites. Chemical Geology 332–333, 45–64.
Hanningan, R., Brookfield, M.E., Basu, A.R., 2010. A detailed ^{87}Sr/^{86}Sr isotope curve for the mid-Cincinnatian (Upper Katian–Lower Hirnantian, Upper Ordovician), NE North American Shelf (Ontario, Canada) transition to the Hirnantian glaciation. Chemical Geology 277, 336–344.
Hippler, D., Buhl, D., Witbaard, R., Richter, D.K., Immenhauser, A., 2009. Towards a better understanding of magnesium isotope ratios from marine skeletal carbonates. Geochimica et Cosmochimica Acta 73, 6134–6146.
Huang, F., Chen, L., Wub, Z., Wang, W., 2013. First-principles calculations of equilibrium Mg isotope fractionations between garnet, clinopyroxene, orthopyroxene, andolivine: implications for Mg isotope thermometry. Earth and Planetary Science Letters 367, 61–70.
Immenhauser, A., Buhl, D., Richter, D.K., Niedermayr, A., Riechelmann, D., Dietzel, M., Schulte, U., 2010. Magnesium-isotope fractionation during low-Mg calcite precipitation in a limestone cave—field study and experiments. Geochimica et Cosmochimica Acta 74, 4346–4364.
Jacobson, A.D., Zhang, Z., Lundstrom, C., Huang, F., 2010. Behavior of Mg isotopes during dedolomitization in the Madison Aquifer, South Dakota. Earth and Planetary Science Letters 297, 446–452.
James, N.P., Stevens, R.K., Barnes, C.R., Knight, I., 1989. Evolution of a lower Paleozoic continental-margin carbonate platform, northern Canadian Appalachians. Special Publication - Society of Economic Paleontologists and Mineralogists 44, 123–146.
Knight, I., James, N.P., 1987. Stratigraphy of the St. George Group (Lower Ordovician), western Newfoundland: the interaction between eustasy and tectonics. Canadian Journal of Earth Sciences 24, 1927–1952.
Knight, I., Azmy, K., Greene, M., Lavoie, D., 2013. Lithostratigraphic setting of diagenetic, isotopic, and geochemistry studies of Ibexian and Whiterockian carbonates of the St. George and Table Head groups in western Newfoundland. Current Research Newfoundland and Labrador (in press).
Knight, I., Azmy, K., Boyce, D., Lavoie, D., 2008. Tremadocian carbonates of the lower St. George Group, Port au Port Peninsula, western Newfoundland: Lithostratigraphic setting of diagenetic, isotopic, and geochemistry studies. Current Research Newfoundland and Labrador Department of Natural Resources Geological Survey. Report 08–1, pp. 1–43.
Land, L.S., 1983. The application of stable isotopes to studies of the origin of dolomite and to problems of diagenesis of clastic sediments. In: Arthur, M.A., Anderson, T.F., Kaplan, I.R., Veizer, J., Land, L.S. (Eds.), Stable Isotopes in Sedimentary Geology. SEPM Short Course Notes, 10, pp. 4-1–4-22.
Lavoie, D., Jackson, S., Girard, I., 2010. Mg isotopes in high temperature saddle dolomites from the Lower Paleozoic of Eastern Canada: significance for the source of magnesium and their origin. AAPG (Abstr.), New Orleans, April 12–14.
Li, W., Chakraborty, S., Beard, B., Romanek, C.S., Johnson, C.M., 2012. Magnesium isotope fractionation during precipitation of inorganic calcite under laboratory conditions. Earth and Planetary Science Letters 333–334, 304–316.
Liu, S.-A., Teng, F.-Z., Yang, W., Wu, F.-Y., 2012. High-temperature interimineral magnesium isotope fractionation in mantle xenoliths from the North China craton. Earth and Planetary Science Letters 308, 131–140.
Machel, H.G., Mountjoy, E.W., 1986. Chemistry and environments of dolomitization: a reappraisal. Earth-Science Reviews 23, 175–202.
Machel, H.G., Mountjoy, E.W., 1990. Coastal mixing zone dolomite, forward modelling, and massive dolomitization of platform-margin carbonate: Discussion. Journal of Sedimentary Petrology 60, 1008–1012.
Mavromatis, V., Gautier, Q., Bosc, O., Schott, J., 2013. Kinetics of Mg partition and Mg stable isotope fractionation during its incorporation in calcite. Geochimica et Cosmochimica Acta 114, 188–203.
McLennan, S.M., 1989. Rare earth elements in sedimentary rocks: influence of provenance and sedimentary processes. In: Lipin, B.R., McKay, G.A. (Eds.),

Geochemistry and Mineralogy of Rare Earth Elements. Mineral. Soc. Am. Rev. Miner, 21, pp. 169–200.
Munnecke, A., Calner, M., Harper, D.A.T., Servais, T., 2010. Ordovician and Silurian sea-water chemistry, sea level, and climate: a synopsis. Palaeogeography, Palaeoclimatology, Palaeoecology 296, 389–413.
Mussman, W.J., Read, J.G., 1986. Sedimentology and development of a passive margin unconformity: Middle Ordovician Knox Unconformity, Virginia Appalachians. Bulletin of the Geological Society of America 97, 282–295.
Pogge von Strandmann, P.A.E., Elliott, T., Marschall, H.R., Coath, C., Lai, Y.-J., Jeffcoate, A.B., Ionov, D.A., 2011. Variations of Li and Mg isotope ratios in bulk chondrites and mantle xenoliths. Geochimica et Cosmochimica Acta 75, 5247–5268.
Pokrovsky, B.G., Mavromatis, V., Pokrovsky, O.S., 2011. Co-variation of Mg and C isotopes in late Precambrian carbonates of the Siberian Platform: a new tool for tracing the change in weathering regime? Chemical Geology 290, 67–74.
Pratt, B.R., James, N.P., 1986. The tidal flat island model for peritidal shallow-upward sequences; St. George Group, western Newfoundland. Sedimentology 33, 313–344.
Riechelmann, S., Buhl, D., Schröder-Ritzrau, A., Spötl, C., Riechelmann, D.F.C., Richter, D.K., Kluge, T., Marx, T., Immenhauser, A., 2012. Hydrogeochemistry and fractionation pathways of Mg isotopes in a continental weathering system: lessons from field experiments. Chemical Geology 300-303, 109–122.
Rustad, J.R., Casey, W.H., Yin, Q.-Z., Bylaska, E.J., Felmy, A.R., Bogatko, S.A., Jackson, V.E., Dixon, D.A., 2010. Isotopic fractionation of Mg^{2+} (aq), Ca^{2+} (aq), and Fe^{2+} (aq) with carbonate minerals. Geochimica et Cosmochimica Acta 74, 6301–6323.
Schauble, E.A., 2011. First-principles estimates of equilibrium magnesium isotope fractionation in silicate, oxide, carbonate and hexaquamagnesium (2+) crystals. Geochimica et Cosmochimica Acta 75, 844–869.
Shaw, H.F., Wasserburg, G.J., 1985. Sm–Nd in marine carbonates and phosphates: implications for Nd isotopes in seawater and crustal ages. Geochimica et Cosmochimica Acta 49, 503–518.
Shepherd, T.J., Rankin, A.H., Alderton, D.H.M., 1985. A Practical Guide to Fluid Inclusions. Blackie, London (239 pp.).
Shields, G.A., Veizer, J., 2004. Isotopic signatures. In: Webby, B.D., Droser, M.L., Paris, F., Percival, I.G. (Eds.), The Great Ordovician Biodiversification Event. Columbia University Press, New York, pp. 68–71.
Shields, G.A., Carden, G.A.F., Veizer, J., Meidla, T., Rong, J.-Y., Li, R.-Y., 2003. Sr, C, and O isotope geochemistry of Ordovician brachiopods: a major isotopic event around the Middle–Late Ordovician transition. Geochimica et Cosmochimica Acta 67, 2005–2025.
Sibley, D.F., 1982. Origin of common dolomite fabrics: clues from the Pliocene. Journal of Sedimentary Petrology 52, 1087–1100.
Stanley, S.M., 2008. Effects of global seawater chemistry on biomineralization: past, present, and future. Chemical Reviews 108, 4483–4498.
Stenzel, S.R., Knight, I., James, N.P., 1990. Carbonate platform to foreland basin: revised stratigraphy of the Table Head Group (Middle Ordovician), western Newfoundland. Canadian Journal of Earth Sciences 27, 14–26.
Teng, F.-Z., Li, W.-Y., Ke, S., Marty, B., Dauphas, N., Huang, S., Wu, F.-Y., Pourmand, A., 2010. Magnesium isotopic composition of the Earth and chondrites. Geochimica et Cosmochimica Acta 74, 4150–4166.
Tipper, E.T., Galy, A., Bickle, M.J., 2006a. Evidence for a fractionated reservoir of Ca and Mg on the continents: implications for the oceanic Ca cycle. Earth and Planetary Science Letters 247, 267–279.
Tipper, E.T., Galy, A., Gaillardet, J., Bickle, M.J., Elderfield, H., Carder, E.A., 2006b. The magnesium isotope budget of the modern ocean: constraints from riverine magnesium isotope ratios. Earth and Planetary Science Letters 250, 241–253.
Tipper, E., Louvat, P., Capmas, F., Galy, A., Gaillardet, J., 2008. Accuracy of stable Mg and Ca isotope data obtained by MC–ICP-MS using the standard addition method. Chemical Geology 257, 65–75.
Tipper, E.T., Gaiullardet, J., Louvat, P., Campas, F., White, A.F., 2010. Mg isotope constraints on soil pore-fluid chemistry: evidence from Santa Cruz, California. Geochimica et Cosmochimica Acta 47, 3883–3896.
Veizer, J., 1983. Chemical diagenesis of carbonates: theory and application of trace element technique. In: Arthur, M.A., Anderson, T.F., Kaplan, I.R., Veizer, J., Land, L.S. (Eds.), Stable Isotopes in Sedimentary Geology. Society of Economic Paleontologists and Mineralogists (SEPM) Short Course Notes, 10, pp. III-1–III-100.
Veizer, J., Ala, D., Azmy, K., Bruckschen, P., Bruhn, F., Buhl, D., Carden, G., Diener, A., Ebneth, S., Goddris, Y., Jasper, T., Korte, C., Pawellek, F., Podlaha, O., Strauss, H., 1999. $^{87}Sr/^{86}Sr$, $\delta^{18}O$ and $\delta^{13}C$ evolution of Phanerozoic seawater. Chemical Geology 161, 59–88.
Wang, Z., Hu, P., Gaetani, G., Liu, Chao, Saenger, C., Cohen, A., Hart, S., 2013. Experimental calibration of Mg isotope fractionation between aragonite and seawater. Geochimica et Cosmochimica Acta 102, 113–123.
Warren, J., 2000. Dolomite: occurrence, evolution, and economically important associations. Earth-Science Reviews 52, 1–81.
Wierzbicki, R., Dravis, J.J., Al-Aasm, I., Harland, N., 2006. Burial dolomitization and dissolution of Upper Jurassic Abenaki platform carbonates, Deep Panuke reservoir, Nova Scotia, Canada. American Association of Petroleum Geologists Bulletin 90, 1843–1861.
Wimpenny, J., Burton, K.W., James, R.H., Gannoun, A., Mokadem, F., Gíslason, S.R., 2011. The behaviour of magnesium and its isotopes during glacial weathering in an ancient shield terrain in West Greenland. Earth and Planetary Science Letters 304, 260–269.
Wombacher, F., Eisenhauer, A., Heuser, A., Weyer, S., 2009. Separation of Mg, Ca and Fe from geological reference materials for stable isotope ratio analyses by MC–ICP-MS and double-spike TIMS. Journal of Analytical Atomic Spectrometry 24, 627–636.
Wombacher, F., Eisenhauer, A., Böhm, F., Gussone, N., Regenberg, M., Dullo, W.C., Rüggeberg, A., 2011. Magnesium stable isotope fractionation in marine biogenic calcite and aragonite. Geochimica et Cosmochimica Acta 75, 5797–5818.
Young, E.D., Galy, A., 2004. The isotope geochemistry and cosmochemistry of Mg. Reviews in Mineralogy and Geochemistry 55, 197–230.
Zhang, S., Barnes, C.R., 2004. Arenigian (Early Ordovician) sea level history and the response of shelf and slope conodont communities, western Newfoundland. Canadian Journal of Earth Sciences 41, 843–865.